https://doi.org/10.15407/ufm.27.02.194

E.M. RUDENKO [1], I.V. KOROTASH [1,], M.V. DYAKIN [1,***], D.Yu. POLOTSKIY [1], S.A. BESPALOV [1,****], O.V. HAMALII [2], N.V. HAMALII [3], and V.A. DEKHTYARENKO [1,4,*****]**

[1] G.V. Kurdyumov Institute for Metal Physics of the N.A.S. of Ukraine, 36 Academician Vernadsky Blvd., UA-03142 Kyiv, Ukraine
[2] State Scientific-Research Institute of Aviation, 6 Kazarmenna Ave., UA-01135 Kyiv, Ukraine
[3] Central Scientific Research Institute of Armament and Military Equipment of Armed Forces of Ukraine, 28 Povitrianykh Syl Ave., UA-03049 Kyiv, Ukraine
[4] E.O. Paton Electric Welding Institute of the N.A.S. of Ukraine, 11 Kazymyr Malevych Str., UA-03150 Kyiv, Ukraine

* rudenko@imp.kiev.ua, emrudenko@ukr.net,
** korotashiv@ukr.net, *** max@imp.kiev.ua, mvdyakin@ukr.net,
**** bespalov@nas.gov.ua, ***** devova@i.ua

ALUMINIUM NITRIDE AS A PROMISING MULTIFUNCTIONAL MATERIAL. Pt. 1. Properties, Crystal Structure, and Production Techniques

A promising material among the nitrides of Group III, namely, aluminium nitride (AlN), is considered. This material is widely used in industry due to its unique properties. Main physical and mechanical properties of AlN, as well as the fields of its application (in acoustic, electronic, and optical devices), are discussed. According to thermodynamic calculations, the Gibbs free energy of the oxidation of metallic aluminium with Al_2O_3 formation is comparatively low, so, it interacts more actively with oxygen than with nitrogen. According to the van 't Hoff equation, the reaction of aluminium with nitrogen is activated, when the partial pressure of nitrogen exceeds significantly the pressure of oxygen; only in this case, aluminium reacts predominantly with nitro-

Citation: E.M. Rudenko, I.V. Korotash, M.V. Dyakin, D.Yu. Polotskiy, S.A. Bespalov, O.V. Hamalii, N.V. Hamalii, and V.A. Dekhtyarenko, Aluminium Nitride as a Promising Multifunctional Material. Pt. 1. Properties, Crystal Structure, and Production Techniques, *Progress in Physics of Metals*, **27**, No. 2: 194–220 (2026)

© Publisher PH "Akademperiodyka" of the NAS of Ukraine, 2025. This is an open access article under the CC BY-ND license (https://creativecommons.org/licenses/by-nd/4.0)

gen and the AlN chemical compound is formed. The ways to reduce the negative impact of oxygen on the process of aluminium-nitride formation are discussed. The main techniques for manufacturing aluminium nitride, in particular, thin films, are considered; their main advantages and disadvantages are surveyed. As shown, based on the main mechanism of chemical reaction between the initial components, the manufacturing techniques are divided into six complex groups. Depending on the conditions of formation, aluminium nitride can have four modifications: (i) a wurtzite structure with a band gap width of 6.2 eV; (ii) a layered hexagonal structure with a band gap width of 3.44 eV; (iii) a zinc-blende structure with a band gap width of 3.24 eV; (iv) a rock-salt structure with a band gap width of 4.04 eV. The features of these types of AlN structure are analysed.

Keywords: aluminium nitride, manufacturing techniques, crystal structure, thin-film coating, physical and mechanical properties.

1. Introduction

According to the literature [1], aluminium nitride (AlN) was first synthesised by J.W. Mallet in 1877. However, it is believed that aluminium nitride was discovered by F. Briegleb and A. Geuther in 1862 [2]. Aluminium nitride is a ceramic material with excellent properties. Although aluminium nitride was first synthesised in the 19th century, its practical application began only a century later [3, 4], and today, the range of its applications continues to expand [5–8] (for a century, it was used only as a nitrogen-fixing agent and fertiliser).

Aluminium nitride (AlN), which has outstanding mechanical, optical, and electronic properties, is widely used in various industries. According to Refs. [6, 9], aluminium nitride is an insulator with a wide band gap (of 6.2 eV), while the mobility of charge carriers does not exceed 1–10 $cm^2/(V \cdot s)$, that causes the high insulating properties of this material [10]. The temperature dependence of AlN conductivity is typical for dielectrics or semiconductors: conductivity increases with temperature. At 20, 400, 500, 600, 800, 1000, 1100, and 1200 °C, the electrical resistance of sintered AlN is of 10^{15}, $2.25 \cdot 10^{13}$, 10^{11}, $8 \cdot 10^9$, $4 \cdot 10^8$, 10^7, $4 \cdot 10^6$, $9 \cdot 10^5$ Ohm·m, respectively [10]. Aluminium nitride has a high specific resistance (of 10^{13} W·cm), relative dielectric permeability (of 8.5), and low linear thermal expansion coefficient (of $4.03 \cdot 10^{-6}$ K^{-1} at 300–500 K and $5.64 \cdot 10^{-6}$ K^{-1} at 500–1300 K), close to that of silicon. Besides, AlN has high thermal stability (up to 2400 K in an inert atmosphere; oxidation in air begins at 1200 K), hardness (of 9 on the Mohs scale), and corrosion resistance in many aggressive environments (*e.g.*, in molten metals and their salts). Due to its piezoelectric properties, AlN is also widely used in microwave acoustic resonators [11]. In addition, aluminium nitride is considered to be one of the most promising materials for effective heat conductors in microelectronic devices due to its high thermal conductivity (390 $W \cdot m^{-1} \cdot K^{-1}$ for perfect crystals) at room temperature, low relative

dielectric permeability ($\varepsilon_r \cong 9$ at 1 MHz), and low dielectric losses ($tg\delta \cong \cong 10^{-4}$ at 1 MHz). The dielectric permeability of AlN increases with temperature; this increase is less pronounced at higher frequencies [10]

These properties and one of the highest thermal conductivity coefficients for thin films (for high-quality AlN films, the thermal conductivity coefficient reaches 120 $W \cdot m^{-1} \cdot K^{-1}$ at room temperature) allow AlN to be used for dissipating excess heat from powerful electronic devices (*e.g.*, powerful LEDs — light-emitting diodes). Besides, AlN can be used as an effective thermal interface material (TIM), when forming thermal interface contacts between the conductive surfaces of electronic devices and functional polymer substrates [12–16].

AlN thin coatings on flexible polymer substrates are promising for the development of multiband blocking filters in the infrared spectrum range [17–19].

Besides, as noted in Ref. [6], aluminium nitride is an effective protective barrier layer that reduces hydrogen permeability (*e.g.*, into titanium), especially under low-pressure conditions [20–24].

2. Thermodynamic Analysis

According to thermodynamic calculations performed in Ref. [25] for 0–1200 °C, the Gibbs free energy for reactions of aluminium with oxygen and nitrogen is negative (Fig. 1). Therefore, both of these reactions can occur spontaneously. However, the Gibbs free energy for the oxidation of metallic aluminium with Al_2O_3 formation is lower, so aluminium interacts more actively with oxygen than with nitrogen [26, 27]. The corresponding equations are [25] as follow:

$$2Al + N_2(g) \rightarrow 2AlN,\ \Delta G_1^{\theta} = -429.86\ \text{kJ/mole (700 °C)};$$

$$2Al + 1.5O_2(g) \rightarrow Al_2O_3,\ \Delta G_2^{\theta} = -1369.96\ \text{kJ/mole (700 °C)}.$$

The authors of Ref. [25] noted that, according to the van 't Hoff equation for thermodynamic isotherms, the reaction of aluminium with nitrogen is activated when the partial pressure of nitrogen significantly exceeds the pressure of oxygen, and then $DG_1^0 < DG_2^0$. Only in this case, aluminium reacts with nitrogen to form the AlN compound.

There are data [27–30], according to which the formation of the AlN phase can be facilitated (an increase in mass fraction yield). Based on thermodynamic calculations, it was shown in Refs. [27, 28] that the presence of a certain amount of magnesium in the system leads to a significant reduction in the partial pressure of oxygen and thereby activation of the aluminium nitride synthesis. According to Ref. [29], the optimal Mg amount for stimulating the aluminium nitriding ranges from 0.1 to 1.0 wt.%.

In Ref. [27], based on the data of Ref. [30], another method for improving the formation of aluminium nitride AlN was proposed. The author

of Ref. [27] showed that the use of ammonia (NH_3) instead of pure nitrogen significantly enhanced the nitriding reaction during the synthesis of aluminium nitride. According to Ref. [30], this is explained by the instability of ammonia, which can dissociate relatively easily into nitrogen and hydrogen when heated above 300 °C. Hydrogen released due to ammonia molecule dissociation is an effective oxygen getter in the system [31].

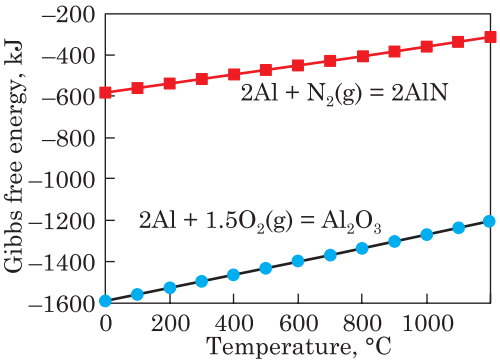

Fig. 1. Gibbs free energy of Al reacting with O and Ni [25]

3. Methods for Producing Aluminium Nitride

In Ref. [32], the main techniques for producing aluminium nitride are considered; their main advantages and disadvantages are discussed. The authors classified these techniques based on the main mechanism of chemical reaction between initial components, which allowed them to distinguish five complex groups and combine methods with a mixed type of chemical reaction into a separate sixth group.

• *Recovery of aluminium oxide during contact with nitrogen or nitrogen-containing substances [33, 34].* This process is schematically shown in Fig. 2.

• *Reaction of aluminium with a liquid or gaseous phase in the form of vapour with a gaseous nitrogen-containing compound [35, 36].* According to Ref. [35], the formation of aluminium nitride in this reaction proceeds as follows: first, a liquid phase forms on the surface of the aluminium particle, and then it reacts with gaseous nitrogen to form a layer of aluminium nitride on the surface.

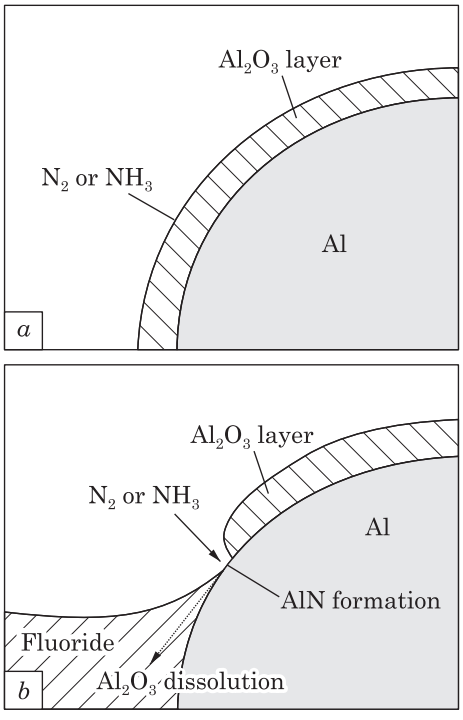

Fig. 2. Schematic illustration of the reaction interface as estimated (*a*) without a flux and (*b*) with a flux (molten fluoride) [34]

The process diagram proposed in Ref. [35] is similar to the scheme shown in Fig. 2.

• *Reaction in the gas phase of a volatile inorganic aluminium compound with nitrogen or nitrogen-containing gases [37, 38].* This technique is based on the exchange reaction [37]. As an example, this is the reaction between $AlCl_3$ and Ca_3N_2, which leads to the formation of 'phase-pure' aluminium nitride (AlN) in a matter of seconds. The by-product of this reaction, $CaCl_2$ salt, whose formation causes this highly exothermic reaction, is simply washed away after the reaction is complete.

• *Reaction of inorganic aluminium compounds with nitrogen-containing organic compounds [39–41].* This technique for producing aluminium nitride involves several stages [31]: (i) pyrolysis of an inorganic aluminium compound (*e.g.*, $Al(OH)_3$) to obtain aluminium oxide Al_2O_3; (ii) mixing aluminium oxide with carbon, which acts as a precursor for the synthesis of aluminium nitride; (iii) reaction of the produced mixture with a nitrogen-containing environment.

• *Reaction of aluminium-containing organic compounds with nitrogen-containing organic compounds or nitrogen [42, 43].* In these reactions, organic aluminium compounds (*e.g.*, $Al(OH)(C_{n+2}H_{2n}O_4)_xH_2O$) are used as initial materials to produce aluminium oxide, with the subsequent addition of urea and glucose [43]. The following steps are the same as in the previous method.

• *Combined techniques for producing aluminium nitride [44].*

Besides, the authors of [32] showed that aluminium nitride produced even with the techniques of the same group can have significantly different physical and mechanical properties, composition, and manufacturing costs. Although each of the proposed techniques has already found its specific use in industry, the following applications are considered the most common: direct reaction between metallic aluminium and a nitrogen-containing environment [45–47] and carbothermal reduction of aluminium oxide in a nitrogen atmosphere [48, 49]. Let us take a closer look at these most commonly used techniques.

Based on data from Ref. [45], the authors of work [46] noted that complete conversion of aluminium into nitride could be achieved using direct nitriding of aluminium powder by heating it to 1600 °C in a nitrogen-containing environment. As shown in Refs. [50–52], the temperature of this reaction can be reduced to 1000 °C by adding KCl or NH_4Cl compounds to nitrogen. This is possible due to the following factors: the formation of voids as a result of KCl evaporation; the reaction between gaseous nitrogen and aluminium chloride vapour formed during the decomposition of NH_4Cl.

In Ref. [46], x-ray phase analysis was used to describe in detail the mechanism of aluminium nitride formation during direct nitriding of aluminium powder (Fig. 3). It was noted that at temperatures up to 500 °C, no reaction occurred between aluminium powder and gaseous nitrogen. When

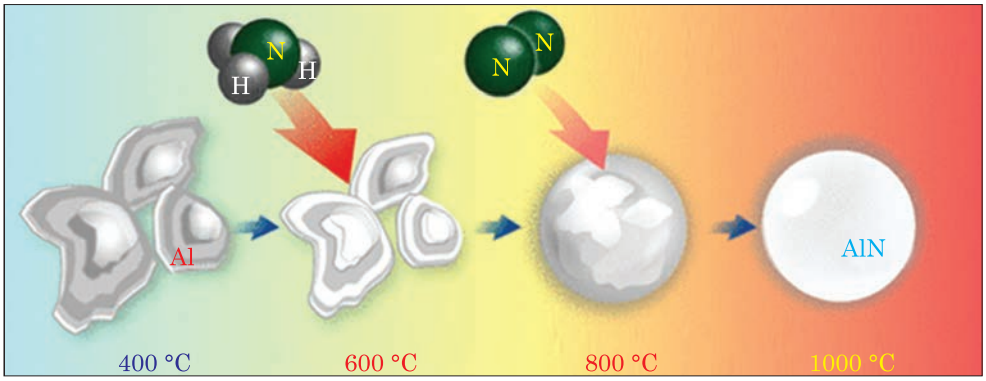

Fig. 3. Formation of aluminium nitride when aluminium powder is heated in an ammonia environment (scheme) [46]

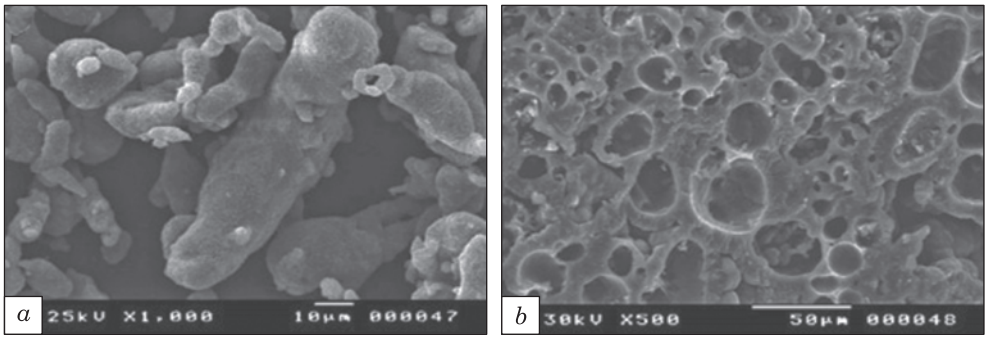

Fig. 4. SEM micrograph of (*a*) starting Al powder and (*b*) AlN powder obtained from direct nitridation of pure Al powder [51]

the temperature rose to 600 °C, aluminium nitride just started to form, but the percentage of this compound was insignificant. When the temperature was raised to 900–1000 °C, the percentage of aluminium powder converted to nitride significantly increased.

The reaction of aluminium nitride formation during heating from 600 to 1000 °C occurs as follows [46]. Above the melting point (660 °C) of aluminium powder (Fig. 4, *a*), particles coagulate and form molten spheres (Fig. 3), while nitride scale forms on their surfaces, which completely covers the aluminium particles [53, 54]. With a further temperature rise, the internal pressure increases due to the melting of unreacted aluminium, which leads to the breaking of the formed scale (shell). When the scale is broken, aluminium flows out in a capillary-like manner and reacts instantly with gaseous nitrogen.

In Refs. [51, 52], the formed consolidated microstructure is indicated as the main disadvantage of the above technique for producing aluminium nitride (Fig. 4, *b*). Since the structure formed can prevent gaseous nitro-

gen from accessing unreacted aluminium particles, the nitriding reaction does not complete. It is possible to reach a volume fraction of aluminium nitride up to 90%.

As is well known, the basic principle of carbothermal reduction consists of heating a mixture of aluminium oxide and carbon in a nitrogen atmosphere above 1600 °C [55]. The reaction of aluminium oxide conversion into nitride occurs according to the formula [49]

$$Al_2O_3(s) + 3C(s) + N_2(g) \overset{>1600\ ^\circ C}{\rightarrow} 2AlN(s) + 3CO(g).$$

As noted in Ref. [56], aluminium nitride powder synthesised using the carbothermal reduction process has better properties in terms of purity, sintering, and moisture resistance compared to other manufacturing techniques. However, the main drawback of this technique, which seriously limits its application in industry, is the high-energy consumption caused by prolonged exposure to high temperatures [57]. Therefore, reducing the synthesis temperature remains an important area for research of the process of carbothermal reduction of aluminium oxide.

As is known, it is practically impossible to reduce the synthesis temperature of the carbothermal reduction by adjusting the sources of carbon and nitrogen in terms of their cost and functionality [49]. Therefore, the enhancement of the reactivity of aluminium oxide (Al_2O_3) powder is considered the most promising way to reduce the synthesis temperature. Based on the literature data [58–62], three main approaches were specified in Ref. [49]:

• reducing the particle size of the aluminium oxide (Al_2O_3) powder by ball milling [58];

• reducing the activation energy of the aluminium oxide (Al_2O_3) powder surface through the use of alkaline earth and/or rare earth compounds, such as CaF_2, $CaCO_3$, $Ca(OH)_2$, $Ca(OH)_2$, CaC_2, Y_2O_3, Yb_2O_3, Y_2O_3–CaO, Y_2O_3–CaO–Li_2O [59, 60];

• use of inorganic aluminium compounds $Al(OH)_3$ or AlOOH, or transition aluminium oxides γ-Al_2O_3, δ-Al_2O_3, θ-Al_2O_3 instead of α-Al_2O_3 powder as initial material [61, 62].

Based on Refs. [63, 64], the authors of Ref. [49] explained, why the use of aluminium oxide Al_2O_3 with different structures significantly affects its ability to transform into an intermediate phase Al–O–N. As known, the α-Al_2O_3 phase is the most stable among all aluminium oxides and belongs to the trigonal system; in this phase, each aluminium atom is co-ordinated with six neighbouring O atoms, forming AlO_6. The η-Al_2O_3 phase belongs to the cubic system with a spinel-type lattice, in which 51% of aluminium atoms are co-ordinated as AlO_6, 36% as AlO_4, and 13% as AlO_3. The θ-Al_2O_3 phase belongs to the monoclinic system with a distorted spinel-type lattice, in which 50% of aluminium atoms are co-ordinated as AlO_6, and 50% of Al atoms are co-ordinated as AlO_4 [63]. Although the

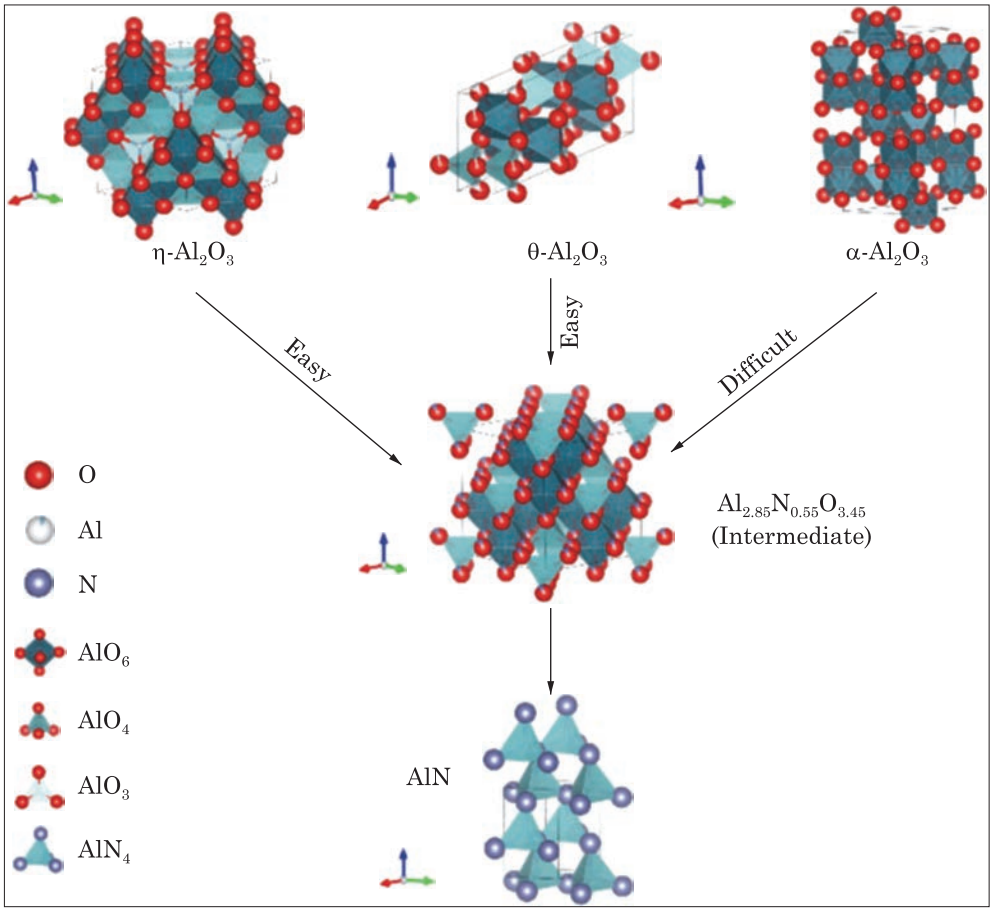

Fig. 5. Transformation of crystal structure during reduction and nitridation reduction [49]

Al–O bond in AlO_4 is shorter and has a higher bond energy than in AlO_6, the nitrogen atom replacing the oxygen atom in AlO_4 needs less energy for the formation of Al–O–N [64] (Fig. 5). Thus, based on the changes in energy, the η-Al_2O_3 and θ-Al_2O_3 phases can easier form an intermediate Al–O–N phase at low temperatures, thereby reducing the overall temperature of aluminium nitride synthesis.

4. Crystal Structure of Aluminium Nitride

The crystal structure of aluminium nitride was first described by Heinrich Otto in 1924 [65]. He discovered that aluminium nitride has a wurtzite-type structure ($a = b \neq c$) with crystal lattice parameters a ranging from 0.3110 to 0.3113 nm and c ranging from 0.4978 to 0.4982 nm, so that the ratio c/a remains ≈1.60 [66]. This structure is considered the most ther-

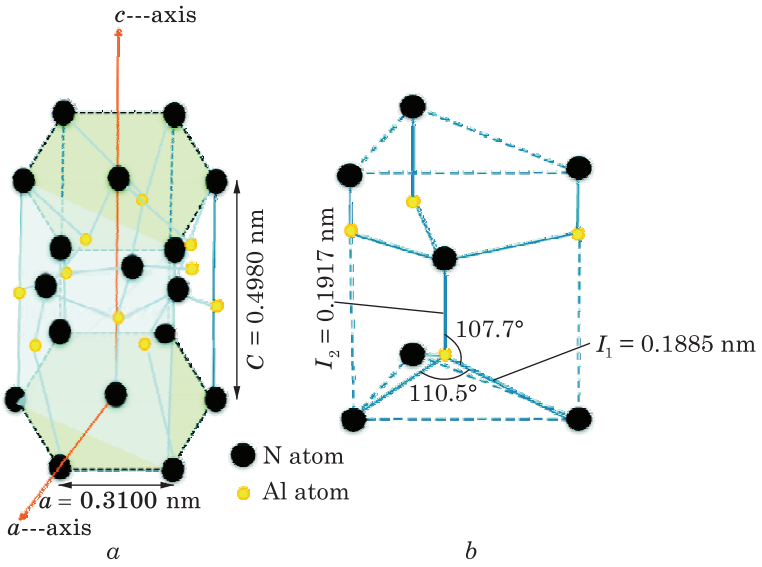

Fig. 6. (*a*) illustrates the hexagonal lattice structure and the *a*, *c* axes, which are parallel to planes (001) and (100), respectively, and (*b*) illustrates the covalent bond angle and length between Al and N atoms and the tetrahedron structures [67]

modynamically stable [67–71]. According to Ref. [69], aluminium nitride has a noncentrosymmetrical wurtzite-type crystal structure with only one axis of symmetry (Fig. 6, *a*). Due to the absence of a centre of symmetry, the centres of positive and negative charges separate under external stress due to lattice deformation, and a dipole moment forms causing piezoelectric polarisation. Due to the large difference in electronegativity between nitrogen and aluminium atoms, the distribution of the electron cloud outside the nucleus is distorted in the aluminium nitride cell. As a result, the positive centre formed by the nucleus and the negative centre formed by the electron cloud do not overlap and form an electric moment. This polarisation effect is called spontaneous polarisation.

In Ref. [72], the formation of aluminium nitride at the electronic level is described. In its unexcited state, aluminium has three electrons in its valence shell distributed as $3s^2 3p^1$. Therefore, the *s* sublevel is occupied with two electrons. The *p* sublevel is half-filled, and there are two unoccupied *p* sublevels, as shown in Fig. 7, *a*. The nitrogen atom has five electrons in its valence shell, which are distributed as $2s^2 2p^3$. The *s* sublevel is occupied with two electrons, and three sublevels p_x, p_y, and p_z are half-filled with one electron each (Fig. 7, *b*). When aluminium transits into an excited state, the $3s^2 3p^1$ sublevels transform to four hybrid $3sp^3$ sublevels, in which three sublevels are half-filled with one electron each, and the rest of the $3sp^3$ sublevels remain unoccupied (Fig. 7, *a*). In nitrogen, the $2s^2 2p^3$ sublevels transform to four hybrid $2sp^3$ sublevels, one of which is filled

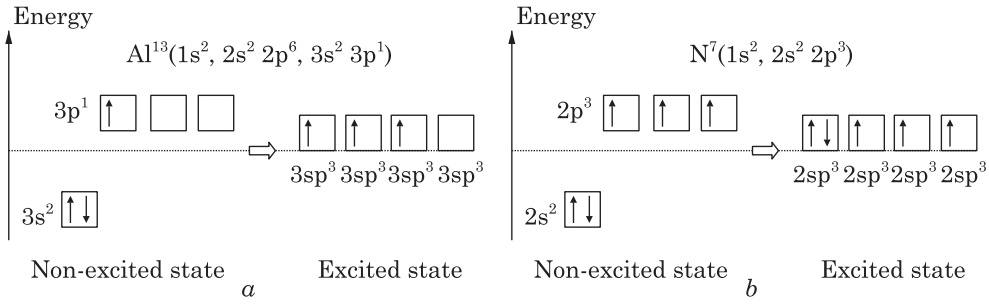

Fig. 7. Hybridisation of aluminium and nitrogen. (*a*) Valence layer in the non-excited state and hybrid sublevels of aluminium, 3*sp*^{3}, in the excited state. (*b*) Valence layer in the non-excited state and hybrid sublevels of nitrogen, 2*sp*^{3}, in the excited state [72]

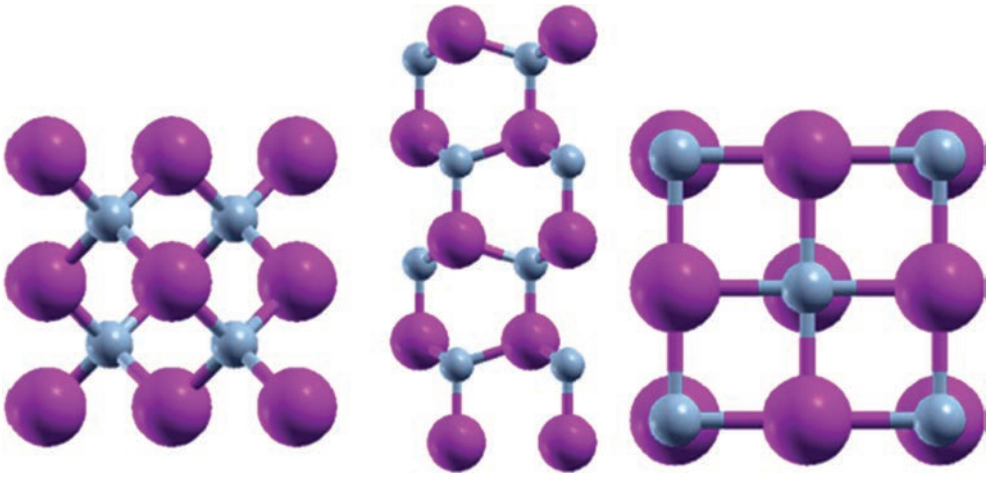

Fig. 8. The AlN crystal structures: left zinc blende (ZB), middle wurtzite (WZ) and right rock salt (rs) (NaCl) [76]

with two 2*sp*^{3} electrons, and three 2*sp*^{3} sublevels are half-filled with one electron each (Fig. 6, *b*). This leads to the formation of covalent bonds between the half-filled sublevels of aluminium and nitrogen atoms [73]. Besides, an additional ionic bond forms between the nitrogen-filled sublevel and the aluminium empty sublevel. The covalent bonds in aluminium nitride have a length of l_1 = 0.1885 nm and form a tetrahedron with an angle of 110.5°. The ionic bond has a length of l_2 = 0.1917 nm, with an angle of 107.7° between the covalent and ionic bonds (Fig. 6, *b*).

According to the literature [74–77], aluminium nitride can have three different modifications, namely: zinc blende (ZB), wurtzite (WZ), and rock salt (NaCl) (Fig. 8). The metastable zinc blende-type phase and the stable wurtzite-type phase can be found in a bulk aluminium nitride at atmospheric pressure, while the rock salt-type phase is stable only at

high pressures of 13–23 GPa [78, 79]. According to Ref. [79], the wurtzite→rock salt phase transformation is accompanied by a 17.9% decrease in volume.

However, based on the data of Refs. [75, 80–85], the authors of Ref. [73] noted that aluminium nitride can exist not in three, but in four modifications:

• wurtzite-type structure (hexagonal lattice with a = 0.3113 nm), space group $P6_3mc$ (prototype is β-ZnS), band gap is of 6.2 eV;

• layered hexagonal structure (hexagonal lattice with a = 0.3290 nm), space group $P6_3/mm3$ (prototype is lh-MgO), band gap is of 3.44 eV; according to Refs. [83, 84, 86], such a structure is observed only in thin films (up to 12 monolayers) and has a larger crystal-lattice parameter compared to the wurtzite-like structure;

• zinc blende structure (cubic lattice with a = 0.4340 nm [84] or a = 0.4406 nm) [65]), space group $F43m$ (prototype is α-ZnS), band gap is of 3.24 eV; the authors of Ref. [73], based on data of Ref. [81], note that this structure is stable only in very thin films, and it transforms into a stable wurtzite-like structure as the film grows;

• rock salt structure (cubic lattice with a = 0.4016 nm [84] or a = 0.4085 nm [65]), space group $Fm3m$ (prototype is NaCl), band gap is of 4.04 eV; as mentioned above, this structure exists only at high pressures.

5. Synthesis of Aluminium-Nitride Coatings

Due to its unique physical and chemical properties [67], aluminium nitride is widely used in industry not only at the macrolevel (powders), but also at the microlevel (coatings) and nanolevel (thin films). The authors of Ref. [67], based on literature data, associate this with the following properties: high piezoelectricity [87]; significant surface acoustic velocity [88]; electromechanical coupling [89]; chemical stability and broad transparency in various spectral ranges [90].

Coating deposition is an iterative process that involves several stages [67]. First, it is necessary to form a gaseous environment from the material (or components of the material) of the targeted coating near the surface of the substrate to which the coating is to be deposited. The physical and chemical properties of this gaseous environment determine the peculiarities of the processes involved in the formation of the coating on the substrate. Then, atoms from this gaseous environment reach the surface of the substrate, where they are adsorbed and migrate across the surface. These atoms collide and combine with other atoms, forming clusters, which eventually transform into comparatively large islands. Through successive iterations of this process, these clusters merge together to form continuous layers. The accumulation of such layers leads to the coating formation [72]. Understanding the physics of each stage of the coating

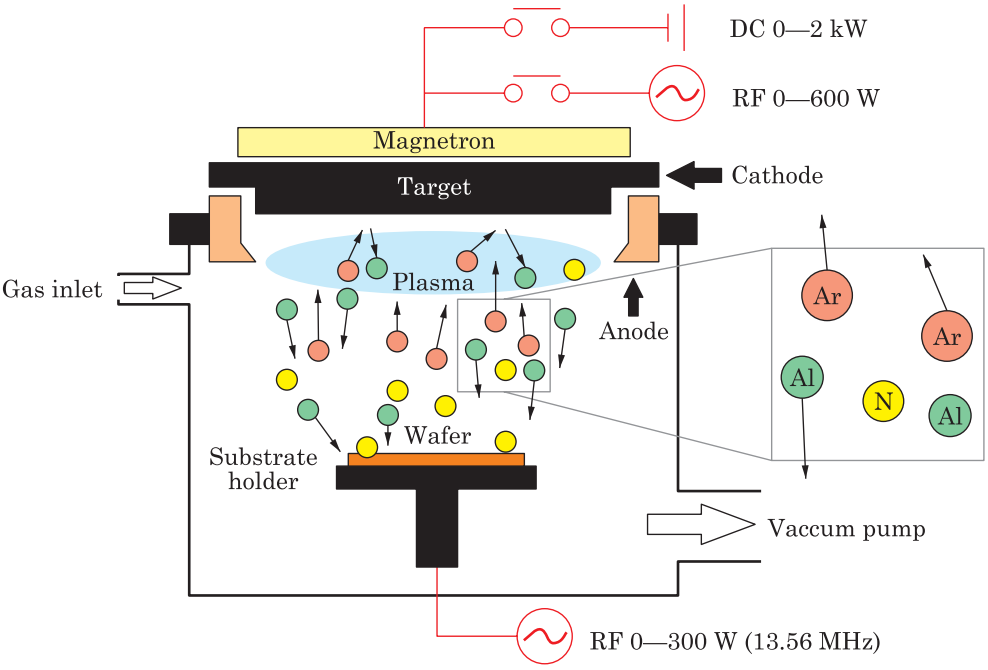

Fig. 9. Reactive sputtering process for AlN film [99, 100]

formation is crucial for optimising its properties, in particular by controlling the deposition parameters.

Obtaining optimal properties of aluminium nitride coatings largely depends on the technique used to produce them. The quality and orientation of the coating significantly affect its efficiency and functionality in specific technological processes [67]. Among various techniques for coating deposition, the following can be distinguished: molecular-beam epitaxy [91]; magnetron sputtering [92]; chemical vapour deposition [93]; vacuum cathodic arc evaporation [94].

Among the abovementioned methods, let us consider vacuum magnetron sputtering and vacuum cathode arc evaporation in more detail, as they allow for excellent control of deposition parameters, low-temperature operation, and compatibility with semiconductor technology.

As shown in Ref. [95], vacuum magnetron sputtering allows for precise control of coating thickness and composition, which is crucial for applications requiring high precision.

Magnetron sputtering has made significant progress since its invention in 1852 [96]. This became possible starting in the 1960s due to the development of various technologies, including plasma technology, vacuum methods, thermal evaporation and spraying. Since then, vacuum magnetron sputtering has evolved from a technique for depositing metal films into a high-tech process with wide industrial applications. It should be

noted that improvements and modifications to this process have significantly enhanced the properties of the coatings and increased the deposition rate [97].

Upon magnetron sputtering (Fig. 9), atoms of material are removed from the target surface by the transfer of momentum caused by collisions with high-energy particles [98]. These interactions lead to various surface phenomena, which may include surface neutralisation, secondary electron emission, ion implantation, and radiation damage. The magnetron sputtering requires a high-quality initial vacuum of at least 10^{-6} Pa to remove water vapour, oxygen, and hydrocarbons that can contaminate the coating. The process occurs at a working gas pressure (usually argon) ranging from 0.1 to 1 Pa to maintain the plasma, which bombards the target and ejects atoms. The energy of particles deposited during sputtering can be relatively high, ranging from 1 to 100 eV.

It is believed that only a few process parameters need to be adjusted to control the growth of aluminium nitride coatings during magnetron sputtering. However, the authors of Refs. [67, 95] note that to improve the control of coating growth parameters during magnetron sputtering, a more comprehensive approach is needed, namely, adjustment of: gas flow ratio (N_2/Ar); sputtering power; substrate temperature; deposition pressure. For example, the N_2/Ar ratio affects the stoichiometry and properties of the coating, while the sputtering power affects the energy of the sputtered atoms and the deposition rate. Maintaining an optimal substrate temperature between 200 and 500 °C increases atomic mobility and promotes the formation of desirable crystal structures. Besides, pressure control allows for better management of the mean free-path length of sputtered particles, which is important for uniform coating growth. Controlling ion bombardment using magnetic field configuration significantly affects coating density and crystal structure perfection.

Certain issues associated with the formation of coatings using magnetron sputtering should be noted. Firstly, it is impossible to predict accurately the structure of the coating due to fluctuations of sputtering parameters [101]. Secondly, the coatings deposited on different substrates have different stress states, which affect their properties [102].

In addition to magnetron sputtering, the vacuum cathode arc evaporation of a target is currently actively used [94]. This deposition technique was first used in 1884 by T.A. Edison, and it was protected by a US patent in 1894 [103]. The main parameters of this method: a current of @ 100 A flows through the plasma on the target surface, while the power density emitted on the target surface reaches @ 10^{13} W/m^2 and corresponds to the temperature of complete ionisation of the material.

A vacuum arc source that generates flows of highly ionised plasma is an effective tool for depositing coatings for various purposes [104–109]. Such coatings form by condensation of a high-energy plasma flow from

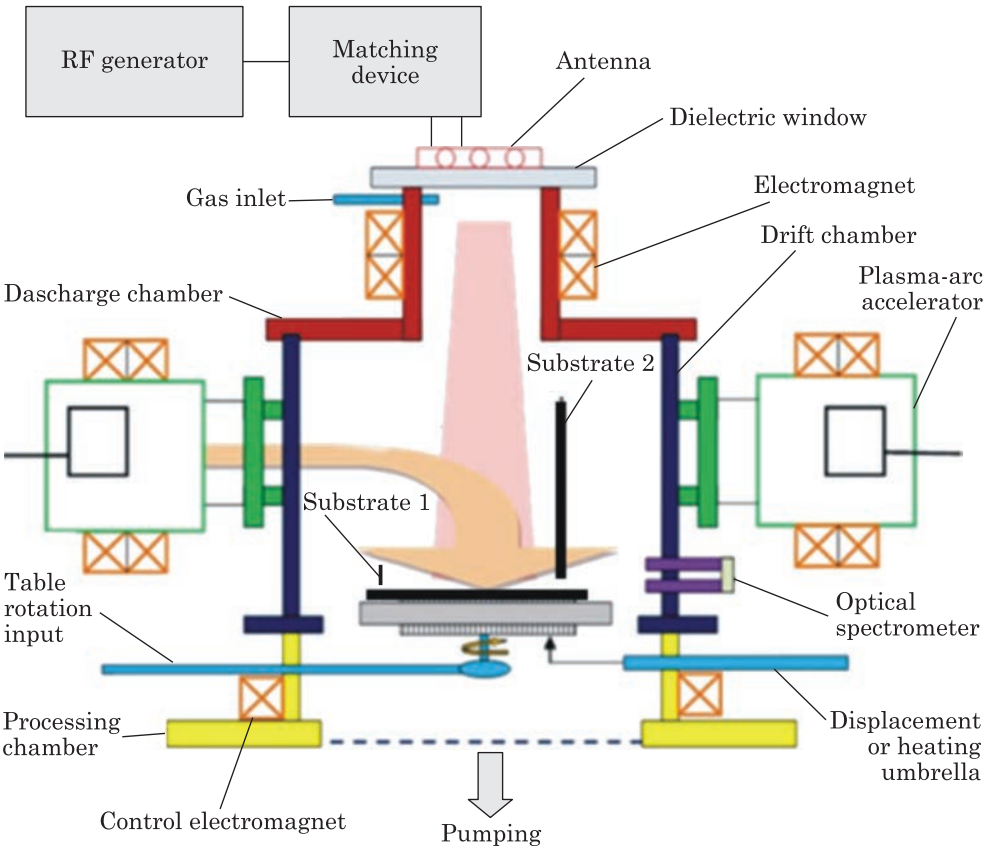

Fig. 10. Scheme of technological process [117, 119, 121]

the cathode on a relatively cold substrate surface. The thickness of the condensate is determined by the plasma flow density and exposure time.

A. Anders [110] provided data on the distribution of ions by the degree of ionisation for all electrically conductive materials. The degree of ionisation of elements in each group and in each period of the periodic table increases with the element number. Forming vapour with a high degree of ionisation and high kinetic energies (up to ≅100 eV) of emitted ions is one of the features of the arc evaporation of the target by cathode spots of a vacuum arc. In Ref. [111], A. Anders provided data on the energies of ions of various target materials. Due to the high pressure of the metal vapour in the spot on the target surface, a jet of metal plasma is ejected in 5–40 ns. If there is an arc stimulator on the surface near the plasma discharge point, such as a dielectric inclusion or a sharp protrusion, a breakdown occurs, and another plasma jet is ejected, and so on. The direct current of the arc is a sequence of short pulses of elementary plasma jets [112] with amplitude of 20–40 A; when this amplitude is exceeded, sev-

eral cathode spots of a vacuum arc form on the target surface. Under a vacuum arc, the main source of plasma is cathode spots [112–116], whose sizes range from a few to several tens of micrometres.

Unique hybrid helicon-arc ion-plasma vacuum equipment was developed at the G.V. Kurdyumov Institute for Metal Physics of the National Academy of Sciences of Ukraine [117–125]. This equipment allows for low-temperature ion-plasma synthesis of coatings [117–125], including aluminium nitride, on flexible thermolabile polymer substrates (Fig. 10).

The developed ion-plasma vacuum equipment has unique technological characteristics [117–125]: low operating temperatures on the substrate of 30–300 °C; a flow of working gas ions from a helicon source with a density on the substrate of 5–10 mA/cm^2; ion energy of 100–150 eV. A vacuum arc accelerator (modernised vacuum arc source) generates an accelerated plasma flow of consumable cathode with a density of up to 10–20 mA/cm^2. The authors of Refs. [119, 121, 122] noted that the plasma density in the chamber of a hybrid helicon-arc reactor reached 10^{11}–10^{13} cm^{-3}, which was several orders of magnitude higher than in magnetrons and typical arc plasma sources.

The developed unit for ion-plasma deposition and ion-plasma modification of surfaces (Fig. 10) includes the following parts [117, 119–123]: a helicon plasma source; a high-frequency pump oscillator with an operating frequency of 13.56 MHz; plasma arc accelerators combined in a single technological reactor chamber. The magnetic system of the helicon plasma source is designed to form conditions for the excitation of natural plasma electromagnetic waves in the discharge plasma, which are known as helicon modes. This creates conditions in the plasma for the effective absorption of external high-frequency energy and the generation of charged working gas particles with high density. The magnetic coil located in the processing chamber directs the plasma flow from the helicon source to the substrate. Besides, this magnetic coil is also used to turn the plasma flow of the consumable cathode material from the plasma arc accelerator toward the substrate. This design of the discharge plasma chamber, which functionally combines two plasma sources (helicon discharge and a plasma arc accelerator), provides a high-quality technological process of forming special coatings (*e.g.*, aluminium nitride).

According to Refs. [117–123], the use of an additional control coil allows controlling plasma flow in the plasma arc accelerator for the first time (Fig. 11).

The process of forming aluminium nitride coatings in a hybrid helicon arc ion-plasma reactor involves the following steps [121].

As seen through the viewing window of the drift chamber, the substrate is placed on the worktable located in the processing chamber at an angle to the bottom plane of the discharge plasma chamber; this angle can be changed depending on the conditions of the experiment. In the first stage, contaminants and water vapour are evacuated from the discharge

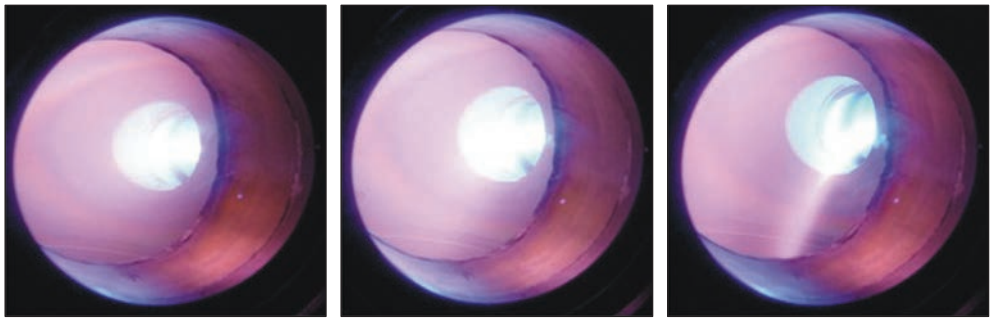

Without rotation | 70-degree rotation | 90-degree rotation

Fig. 11. Plasma flow control in plasma arc accelerator [118, 119, 121]

plasma chamber to a pressure of approximately $5 \cdot 10^{-2}$ Pa, and then an inert working gas (argon) is fed into the chamber. After the chamber is filled with argon, a pressure of 1 Pa is maintained, at which the working gas is ionised by high-frequency energy emitted through an antenna. The antenna is connected *via* an adapter to a high-frequency generator operating at a frequency of 13.56 MHz with a power of 400 W. At this high-frequency power, an inductive discharge occurs in the plasma.

An external magnetic field is applied in the discharge chamber by switching on magnetic coils located outside the chamber, a little bit below the viewing window. This magnetic field causes the transfer and absorption of high-frequency energy in the plasma by its naturally resonant electromagnetic waves excited by the antenna [117, 120–123]. Thus, a helicon wave structure forms in the plasma.

Adjustment of the current supplied to the coils, while maintaining a constant power input, allows controlling the spatial distribution of plasma density. For additional cleaning of the walls of the discharge plasma chamber from contaminants remaining after high-vacuum pumping, the plasma with a volume diffuse discharge is activated throughout the whole chamber. The control magnetic coil, located in the processing chamber area (Fig. 10), forms the plasma flow from the helicon source to the substrate [117, 120–123, 125]. Turning on this magnetic coil causes a discharge in the plasma ('plasma column'). This 'plasma column' discharge is accompanied by intense bombardment of the substrate surface with plasma ions. This allows sputtering the adsorbed light components of the residual environment, which remained on the substrate even after high-vacuum cleaning [117, 120–123, 125].

When all stages of cleaning the substrate and the volume of the plasma discharge chamber are fulfilled (it takes about 15 min), argon is replaced with nitrogen, and the plasma arc accelerator is turned on at a pressure of $5 \cdot 10^{-2}$ Pa. When current is supplied and a magnetic field is applied close to the end face of the cathode of the plasma arc accelerator,

a directed, intense, high-energy plasma flow from the cathode is formed, which is accelerated by a radial electric field up to the energies corresponding to the voltage drop through the discharge [117–121, 123]. This high-energy plasma flow from the cathode enters the drift chamber. The ion flux rotation used to prevent microdroplets from hitting the substrate is provided by activating a control magnetic coil located in the processing chamber. When a current of 0.5 A is applied to the coil, the ion flux is rotated and directed toward the substrate surface (Fig. 11). As a result, the consumable cathode material is deposited onto the substrate.

6. Conclusions

The literature data on the physical and mechanical properties, methods of production, and applications of aluminium nitride are summarised. It is noted that aluminium nitride can exist in four different forms that have different physical, mechanical, optical, and electrodynamic properties. Aluminium nitride is widely used not only at the macrolevel (powders), but also at the micro-level (coatings) and nanolevel (thin films).

The main issue in producing high-quality aluminium nitride (or coatings based on it) is residual oxygen, since aluminium has a much higher affinity for oxygen than for nitrogen. The main ways to enhance the formation of aluminium nitride are as follow:

• introducing magnesium (0.1–1.0 wt.%), which significantly reduces the partial pressure of oxygen and thereby activates the synthesis of aluminium nitride;

• using ammonia (NH_3) instead of pure nitrogen, which is an unstable compound and can easily dissociate into nitrogen and hydrogen (hydrogen released in this reaction effectively binds residual oxygen).

Acknowledgements. The research was partially supported by project No. 4.2/26-P of the budget program of the N.A.S. of Ukraine (КПКВК 6541230).

Authors' Contributions. E.M.R.: supervision of the research, formulation of the main ideas, providing the structure of the manuscript and important comments on the final text. V.A.D.: analysis of the literature data for sections 2 and 3, regarding the synthesis of aluminium nitride; identification of the main techniques for producing AlN; optimisation of manufacturing aluminium nitride based on thermodynamic calculations. I.V.K.: co-leadership in the development of unique helicon arc ion-plasma equipment; proposed the use of AlN film coatings for forming functional devices in the IR range; editing the manuscript. D.Yu.P.: development of equipment and testing of technological processes for helicon arc ion-plasma synthesis of AlN film coatings, description of the technology features (sec. 4). M.V.D.: thermal analysis of the AlN film structures. S.A.B.:

analysis of the AlN crystal structure. O.V.H.: analysis; the use of AlN film coatings for aviation equipment was proposed. N.V.H.: analysis; the use of AlN film coatings for military equipment was proposed. All authors approved the final version of the manuscript.

REFERENCES

1. J.C. Paz de Mattos, L.F. Rodrigues, Й. Marlon de Moraes Flores, and V. Krivan, Determination of Trace Impurities in Aluminum Nitride by Direct Solid Sampling Graphite Furnace Atomic Absorption Spectrometry, *Spectrochim. Acta, Part B: At. Spectrosc.*, **66**, No. 8: 637–643 (2011); https://doi.org/10.1016/j.sab.2011.07.002
2. F. Briegleb and A. Geuther, Ueber das Stickstoffmagnesium und die Affinitäten des Stickgases zu Metallen, *Justus Liebigs Annalen der Chemie.*, **123**, No. 2: 228–241 (1862); https://doi.org/10.1002/jlac.18621230212
3. L. Guo, H.S. Wu, and Z.H. Jin, Magic Behavior and Bonding Nature in Hydrogenated Aluminum Nitride Clusters, *Appl. Surf. Sci.*, **242**: 88–96 (2005); https://doi.org/10.1016/j.apsusc.2004.08.001
4. L. Shen, T. Cheng, L. Wu, X. Li, and Q. Cui, Synthesis and Optical Properties of Aluminum Nitride Nanowires Prepared by arc Discharge Method, *J. Alloys Compds.*, **465**: 562–566 (2008); https://doi.org/10.1016/j.jallcom.2007.11.007
5. B. Sundarapandian, L. Kirste, P. Straňák, M. Prescher, S. Münch, and M. Raghuwanshi, Optical Properties of Aluminum Nitride Thin Films Prepared by Magnetron Sputter Epitaxy, *Phys. Status Solidi A*, **222**: 202500243 (2025); https://doi.org/10.1002/pssa.202500243
6. E.M. Rudenko, M.V. Dyakin, I.V. Korotash, D.Yu. Polotskiy, and V.A. Dekhtyarenko, Helicon-Arc Ion-Plasma Synthesis of AlN-Based Film Coatings on the Steel 3 and Aluminium Substrates, *Metallofiz. Noveishie Tekhnol.*, **47**, No. 7: 703–715 (2025); https://doi.org/10.15407/mfint.47.07.0703
7. Z.-Y. Jiao, S.-H. Ma, and J.-F. Yang, A Comparison of the Electronic and Optical Properties of Zinc-blende, Rocksalt and Wurtzite AlN: A DFT Study, *Solid State Sci.*, **13**, No. 2: 331–336 (2011); https://doi.org/10.1016/j.solidstatesciences.2010.11.030
8. R.T. Bondokov, K. Hogan, G.Q. Norbury, S. Matsumoto, and J. Grandusky, Development of 100 mm AlN Single-Crystal Growth and Subsequent Substrate Preparation *Phys. Status Solidi B*, **262**: 2500032 (2025); https://doi.org/10.1002/pssb.202500032
9. H. Yang, J. Sun, H. Wang, H. Li, and B. Yang, A Review of Oriented Wurtzite-Structure Aluminum Nitride Films, *J. Alloys Compds.*, **989**: 174330 (2024); https://doi.org/10.1016/j.jallcom.2024.174330
10. V.Ya. Shevchenko and S.M. Barinov, *Technical Ceramics* (Moskva: Nauka: 1993).
11. S.T. Haider, M.A. Shah, D.-G. Lee, and S. Hur, A Review of the Recent Applications of Aluminum Nitride-Based Piezoelectric Devices, *IEEE Access*, **11**: 58779–58795 (2023); https://doi.org/10.1109/ACCESS.2023.3276716
12. O.Ye. Pogorelov, O.V. Filatov, E.M. Rudenko, I.V. Korotash, and M.V. Dyakin, Characterization Methods of Heat Flows in Solids, *Prog. Phys. Met.*, **24**, No. 2: 239–281 (2023); https://doi.org/10.15407/ufm.24.02.239

13. E.M. Rudenko, A.O. Krakovnyy, M.V. Dyakin, I.V. Korotash, D.Yu. Polotskiy, and M.A. Skoryk, Cross Thermal Conductivity of Aluminium Nitride Films and Thermal Resistance of AlN/Si and AlN/Al Interfaces, *Metallofiz. Noveishie Tekhnol.*, **44**, No. 8: 989–1002 (2022); https://doi.org/10.15407/mfint.44.08.0989
14. A. Jacquot, B. Lenoir, A. Dauscher, P. Verardi, F. Craciun, M. Stцlzer, M. Gartner, and M. Dinescu, Optical and Thermal Characterization of AlN Thin Films Deposited by Pulsed Laser Deposition, *Appl. Surf. Sci.*, **186**: 507 (2002); https://doi.org/10.1016/S0169-4332(01)00767-X
15. R.L. Xu, M.M. Rojo, S.M. Islam, A. Sood, B. Vareskic, A. Katre, N. Mingo, K.E. Goodson, H.G. Xing, D. Jena, and E. Pop, Thermal Conductivity of Crystalline AlN and the Influence of Atomic-Scale Defects, *J. Appl. Phys.*, **126**: 185105 (2019); https://doi.org/10.1063/1.5097172
16. E. Rudenko, V. Burlakov, I. Korotash, M. Dyakin, D. Polotskiy, and O. Kalenyuk, Effective Thermal Conductivity of Flexible Two-Layer Aluminum Nitride/Polytetrafluoroethylene Structure, *Phys. Status Solidi A*, **222**, No. 10: 2400860 (2025); https://doi.org/10.1002/pssa.202400860
17. E. Rudenko, Z. Tsybrii, F. Sizov, I. Korotash, D. Polotskiy, M. Skoryk, M. Vuichyk, and K. Svezhentsova, Infrared Blocking, Microwave and Terahertz Low-Loss Transmission AlN Films Grown on Flexible Polymeric Substrates, *J. Appl. Phys.*, **121**, No. 13: 135304 (2017); https://doi.org/10.1063/1.4979858
18. Z. Tsybrii, F. Sizov, M. Vuichyk, I. Korotash, and E. Rudenko, AlN and MgO Thin-Layer Coatings on the Bendable Polymeric Substrates as Selective Filters for IR and THz Spectral Ranges, *Infr. Phys. Technol.*, **107**: 103323 (2020); https://doi.org/10.1016/j.infrared.2020.103323
19. F. Sizov, Z. Tsybrii, E. Rudenko, I. Korotash, M Vuichyk, K Svezhentsova, and D. Polotskiy, Reststrahlen Band Infrared Damping, Microwave Transparent AlN/Polymeric Film Filters, *Vacuum*, **225**: 113248 (2024); https://doi.org/10.1016/j.vacuum.2024.113248
20. D. Oryshych, V. Dekhtyarenko, T. Pryadko, V. Bondarchuk, and D. Polotskiy, Protection of Titanium Against Hydrogen Embrittlement, *Machines Technologies Materials*, **13**, No. 12: 561 (2019).
21. T.V. Pryadko, V.A. Dekhtyarenko, V.I. Bondarchuk, M.A. Vasilyev, and S.M. Voloshko, Complex Approach to Protecting Titanium Constructions from Hydrogen Embrittlement, *Metallofiz. Noveishie Tekhnol.*, **42**, No. 10: 1419–1429 (2020); https://doi.org/10.15407/mfint.42.10.1419
22. T.V. Pryadko, V.A. Dekhtyarenko, and A.A. Shkola, Influence of the Ambient Medium in the Course of Laser Treatment on the Resistance of Titanium to Hydrogen Embrittlement, *Mater. Sci.*, **56**: 75–81 (2020); https://doi.org/10.1007/s11003-020-00399-w
23. V.A. Dekhtyarenko, T.V. Pryadko, O.I. Boshko, V.V. Kirilchuk, H.Yu. Mykhailova, and V.I. Bondarchuk, Hydrogen Embrittlement of Titanium: Phenomena and Main Ways of Prevention, *Prog. Phys. Met.*, **25**, No. 2: 276–293 (2024); https://doi.org/10.15407/ufm.25.02.276
24. V.A. Dekhtyarenko, T.V. Pryadko, V.V. Kyrylchuk, M.S. Nizameyev, and V.I. Bondarchuk, Cobalt-Based Alloy Coating for Protecting Titanium from Hydrogen Permeation, *Metallofiz. Noveishie Tekhnol.*, **47**, No. 11: 1185–1198 (2025); https://doi.org/10.15407/mfint.47.11.1185
25. J. Liu, S. Zhang, B. Lou, and H. Shen, Formation of Aluminum Nitride in Dross by Contact-Diffusion Reaction During Aluminum Recycling, *J. Alloys Compds.*, **1010**:

177432 (2025);
https://doi.org/10.1016/j.jallcom.2024.177432
26. C.C. Chen, C.Y. Chen, H.W. Yang, Y.K. Kuo, and J.S. Lin, Phase Equilibrium in Carbothermal Reduction Al_2O_3→AlN Studied by Thermodynamic Calculations, *Atlas J. Mater. Sci.*, **1**, No. 2: 30–37 (2014);
https://doi.org/10.5147/ajms.2014.0172
27. R.G. Reddy, Thermodynamics and Synthesis of AlN-Reinforced Mg Alloy Composites, *Metall. Mater. Trans B*, **55**: 2115–2123 (2024);
https://doi.org/10.1007/s11663-024-03100-7
28. D. Kent, J. Drennan, and G. Schaffer, A Morphological Study of Nitride Formed on Al at Low Temperature in the Presence of Mg, *Acta Mater.*, **59**: 2469–2480 (2011);
https://doi.org/10.1016/j.actamat.2010.12.050
29. S. Huo, M. Qian, G. Schaffer, and E. Crossin, Aluminium Powder Metallurgy, *Fundamentals of Aluminium Metallurgy* (Elsevier: 2011), p. 655–701;
https://doi.org/10.1533/9780857090256.3.655
30. Q. Zheng and R.G. Reddy, Kinetics of *In-situ* Formation of AlN in Al Alloy Melts by Bubbling Ammonia Gas, *Metall. Mater. Trans. B*, **34**: 793–804 (2003);
https://doi.org/10.1007/s11663-003-0085-y
31. W.-S. Jung, Synthesis of Aluminum Nitride Powder from δ-Alumina Nanopowders under a Mixed Gas Flow of Nitrogen and Hydrogen, *Ceramics Int.*, **38**: 871–874 (2012);
https://doi.org/10.1016/j.ceramint.2011.07.002
32. A.A. Elagin, A.R. Beketov, M.V. Baranov, and R.A. Shishkin, Aluminum Nitride. Preparation Methods (Review), *Refract. Ind. Ceram.*, **53**, No. 6: 57–67 (2013);
https://doi.org/10.1007/s11148-013-9546-2
33. M.E. Galvez, A. Frei, F. Meier, and A. Steinfeld, Production of AlN by Carbothermal and Methanothermal Reduction of Al_2O_3 in N_2 Flow Using Concentrated Thermal Radiation, *Ind. Eng. Chem. Res.*, **48**: 528–533 (2009);
https://doi.org/10.1021/ie8011193
34. O. Takeda, K. Takagi, T. Handa, K. Katagiri, H. Zhu, and Y. Sato, Production of Aluminum Nitride from Aluminum Metal Using Molten Fluoride, *J. Mater. Res.*, **30**, No. 5: 635–644 (2015);
https://doi.org/10.1557/jmr.2015.22
35. Y. Qiu and L. Gao, Nitridation Reaction of Aluminum Powder in Flowing Ammonia, *J. Europ. Ceram. Soc.*, **23**: 2015–2022 (2003);
https://doi.org/10.1016/S0955-2219(03)00014-1
36. S. Liao, Rafi ud-din, L. Zhang, A. Chu, Y. Zhao, T. Li, and S. Liang, Optimization of Process Parameters for Preparing AlN Nanopowders by Combining Carbon-Containing Droplet Combustion and Carbothermal Reduction Methods, *Ceram. Int.*, **50**, No. 24: 53183–53192 (2024);
https://doi.org/10.1016/j.ceramint.2024.10.168
37. R.A. Janes, M.A. Low, and R.B. Kaner, Rapid Solid-State Metathesis Routes to Aluminum Nitride, *Inorg. Chem.*, **42**, No. 8: 2714–2719 (2003);
https://doi.org/10.1021/ic026143z
38. V.S. Kudyakova, R.A. Shishkin, A.A. Elagin, M.V. Baranov, and A.R. Beketov, Aluminium Nitride Cubic Modifications Synthesis Methods and Its Features. Review, *J. Eur. Ceram. Soc.*, **37**, No. 4: 1143–1156 (2017);
https://doi.org/10.1016/j.jeurceramsoc.2016.11.051
39. N.R. Fetter, B. Bartocha, F.E. Brinckman Jr., and D.W. Moore, Some Reactions of Organoaluminum Compounds with Nitrogen-Containing Bases, *Canadian J. Chem.*, **41**, No. 5: 1359–1367 (1963);
https://doi.org/10.1139/v63-186

40. T. Mori, T. Kobayashi, Y. Kawanishi, H. Kominami, Y. Nakanishi, and K. Hara, Fabrication of AlN Single Crystal Particles by a Chemical Vapor Method Using Aluminum Chloride, *Phys. Status Solidi C*, **8**: 1459–1462 (2011); https://doi.org/10.1002/pssc.201001115
41. C. Li, C. Xu, Y. Shi, J. Song, P. Du, C. Xie, G. Xue, Z. Chen, L. Wang, and Z. Wang, Effect of Different Phases of Alumina on the Preparation of Aluminum Nitride Powder by Carbothermal Reduction-Nitridation Method, *Ceram. Int.*, **51**, No. 19: 28229–28235 (2025); https://doi.org/10.1016/j.ceramint.2025.04.035
42. K. Ramakrishnaiahand N. Subramanyan, Effect of some Nitrogen Containing Organic Compounds on the Corrosion and Polarization Behaviour of Aluminium in 1M Solutions of Sodium Hydroxide and Hydrochloric Acid with and without Calcium, *Corros. Sci.*, **16**, No. 5: 307–316 (1976); https://doi.org/10.1016/0010-938X(76)90116-5
43. A. Sakthisabarimoorthi, S.M. Lee, S.S. Ryu, and D.H. Yoon, Impact of Various Input Parameters on the Preparation of Different AlN Nanostructures by Hybrid Route of Hydrothermal and Carbothermal Reduction Nitridation Technique, *Korean J. Chem. Eng.*, **41**: 147–155 (2024); https://doi.org/10.1007/s11814-024-00028-1
44. Y. Wang, L. Qiao, J. Zheng, Y. Ying, J. Yu, W. Li, and S. Che, Preparation of AlN with Low Agglomeration Using Polyethylene Glycol and Emulsifier to Disperse the Ultrafine Raw Powders, *Ceram. Int.*, **49**, No. 1: 1390–1400 (2023); https://doi.org/10.1016/j.ceramint.2022.09.120
45. G. Selvaduray and L. Sheet, Aluminium Nitride: Review of Synthesis Methods, *Mater. Sci. Technol.*, **9**: 463-473 (2013); https://doi.org/10.1179/mst.1993.9.6.463
46. T. Kato and K. Sugawara, Low-Temperature Synthesis of Aluminum Nitride by Addition of Ammonium Chloride, *ACS Omega*, **4**, No. 12: 14714–14720 (2019); https://doi.org/10.1021/acsomega.9b01140
47. S. Rogers, M. Dargusch, and D. Kent, Impacts of Temperature and Time on Direct Nitridation of Aluminium Powders for Preparation of AlN Reinforcement, *Materials*, **16**, No. 4: 1583 (2023); https://doi.org/10.3390/ma16041583
48. S.A. Rounaghi, H. Eshghi, S. Scudino, A. Vyalikh, D.E.P. Vanpoucke, W. Gruner, S. Oswald, A.R. Kiani Rashid, M.S. Khoshkhoo, U. Scheler, and J. Eckert, Mechanochemical Route to the Synthesis of Nanostructured Aluminium Nitride, *Sci. Rep.*, **6**: 33375 (2016); https://doi.org/10.1038/srep33375
49. G. Li, B. Li, B. Ren, H. Chen, B. Zhu, and J. Chen, Synthesis of Aluminum Nitride Using Sodium Aluminate as Aluminum Source, *Processes*, **11**, No. 4: 1034 (2023); https://doi.org/10.3390/pr11041034
50. Y. Qiu and L. Gao, Novel Way to Synthesize Nanocrystalline Aluminum Nitride from Coarse Aluminum Powder, *J. Am. Ceram. Soc.*, **86**: 1214–1216 (2004); https://doi.org/10.1111/j.1151-2916.2003.tb03452.x
51. M. Radwan, M. Bahgat, and A.A. El-Geassy, Formation of Aluminium Nitride Whiskers by Direct Nitridation, *J. Eur. Ceram. Soc.*, **26**: 2485–2488 (2006); https://doi.org/10.1016/j.jeurceramsoc.2005.06.033
52. M. Radwan and M. Bahgat, A Modified Direct Nitridation Method for Formation of Nano-AlN Whiskers, *J. Mater. Process. Technol.*, **181**: 99–105 (2007); https://doi.org/10.1016/j.jmatprotec.2006.03.045
53. T. Okada, M. Toriyama, and S. Kanazaki, Synthesis of Aluminium Nitride Sintered Bodies Using the Direct Nitridation of Al Compacts, *J. Eur. Ceram. Soc.*, **20**: 783–787 (2000);

https://doi.org/10.1016/S0955-2219(99)00204-6
54. V. Rosenband and A. Gany, Activation of Combustion Synthesis of Aluminium Nitride Powder, *J. Mater. Process Technol.*, **147**: 179–203 (2004); http://dx.doi.org/10.1016/j.jmatprotec.2003.12.017
55. W. Tang, Y. Yu, Y. Yu, Z. Huang, W. Wang, S. Lin, J. Luo, C. Zhang, and Z. Zhang, Low-Temperature Formation of Aluminum Nitride Powder from Amorphous Aluminum Oxalate *via* Carbothermal Reduction, *Inorganics*, **13**, No. 10: 317 (2025); https://doi.org/10.3390/inorganics13100317
56. Q. Wen, P. Wang, J.W. Zheng, Y. Ying, J. Yu, W.C. Li, S.L. Che, and L. Qiao, Carbothermal Reduction Synthesis of Aluminum Nitride from $Al(OH)_3$/C/PVB Slurries Prepared by Three-Roll Mixing, *Materials*, **14**: 1386 (2021); https://doi.org/10.3390/ma14061386
57. S. Chen, K. Lu, X. Zhou, Z. Zhouchen, X. Huang, J. Qi, and T. Lu, High Sphericity AlN Powder Carbothermal Reduced from Spray Granulated Al_2O_3/C Precursor, *Ceram. Int.*, **51**, No. 6: 7336–7342 (2025); https://doi.org/10.1016/j.ceramint.2024.12.170
58. Z.J. Liu, L.Y. Dai, D.Z. Yang, S. Wang, B.J. Zhang, W.C. Wang, and T.H. Cheng, Synthesis of Aluminum Nitride Powders from a Plasma-Assisted Ball Milled Precursor Through Carbothermal Reaction, *Mater. Res. Bull.*, **61**: 152–158 (2015); https://doi.org/10.1016/j.materresbull.2014.10.015
59. A.L. Molisani and H.N. Yoshimura, Low-temperature Synthesis of AlN Powder with Multicomponent Additive Systems by Carbothermal Reduction–Nitridation Method, *Mater. Res. Bull.*, **45**: 733–738 (2010); https://doi.org/10.1016/j.materresbull.2010.02.012
60. S.M. Lee, M.T. Ayman, S.M. Jang, S. Park, and D.H. Yoon, Synthesis of Pure Fine AlN Powder *via* CRN Using Nitridation Promoter, *Mater. Today Commun.*, **41**: 110935 (2024); https://doi.org/10.1016/j.mtcomm.2024.110935
61. A. Hermawan, H. Son, Y. Asakura, T. Mori, and S. Yin, Synthesis of Morphology Controllable Aluminum Nitride by Direct Nitridation of γ-AlOOH in the Presence of N_2H_4 and Their Sintering Behavior, *J. Asian Ceram. Soc.*, **6**: 63–69 (2018); https://doi.org/10.1080/21870764.2018.1439611
62. S.M. Lin, Y.L. Yu, M.F. Zhong, H. Yang, and Y.C. Qiu, The Activation Mechanism of Oxalic Acid on γ-Alumina and the Formation of α-Alumina, *Ceram. Int.*, **47**: 26869–26876 (2021); https://doi.org/10.1016/j.ceramint.2021.06.096
63. R.S. Zhou and R.L. Snyder, Structures and Transformation Mechanisms of the η, γ and θ-Transition Aluminas, *Acta Cryst. B*, **47**: 617–630 (1991); https://doi.org/10.1107/S0108768191002719
64. Y. Dai, X.M. Min, C.W. Nan, X.M. Pei, and H.L. Ren, Structural Characterization of AION by^{27}Al Mas NMR and Quantum Chemistry Method, *MRS Online Proceedings Library*, **538**: 573–578 (2011); https://doi.org/10.1557/PROC-538-573
65. B. Ahmed and B. I. Sharma, Structural and Electronic Properties of AlN in Rocksalt, Zinc Blende and Wurtzite Phase: A dft Study, *Digest J. Nanomater. Biostruct.*, **16**, No. 1: 125–133 (2021); https://doi.org/10.15251/DJNB.2021.161.125
66. W. Werdecker and F. Aldinger, Aluminum Nitride-An Alternative Ceramic Substrate for High Power Applications in Microcircuits, *IEEE Transactions on Components, Hybrids, and Manufacturing Technology*, **7**: 399–404 (1984); https://doi.org/10.1109/TCHMT.1984.1136380

67. N.A.K. Jadoon, V. Puvanenthiram, M.A.H. Mosa, A. Sharma, and K. Wang, Recent Advances in Aluminum Nitride (AlN) Growth by Magnetron Sputtering Techniques and Its Applications, *Inorganics*, **12**, No. 10: 264 (2024); https://doi.org/10.3390/inorganics12100264
68. J. Zagorac, D. Zagorac, M. Rosić, J.C. Schцn, and B. Matović, Structure Prediction of Aluminum Nitride Combining Data Mining and Quantum Mechanics, *CrystEngComm*, **19**: 5259–5268 (2017); https://doi.org/10.1039/C7CE01039G
69. Z. Liu, W. Li, Z. Qin, L. Jin, Z. Sun, and H. Wu, Research on the Stability of Different Polar Surfaces in Aluminum Nitride Single Crystals, *Crystals*, **14**, No. 4: 337 (2024); https://doi.org/10.3390/cryst14040337
70. L. Wang, J. Cheng, K. Qu, Q. Zhu, B. Tian, and Z. Yang, Aluminum-Nitride-Based Semiconductors: Growth Processes, Ferroelectric Properties, and Performance Enhancements, *Inorganics* **13**, No. 2: 29 (2025); https://doi.org/10.3390/inorganics13020029
71. R. Li, C. Cheng, F. Dong, G. Wu, W. Shen, K. Liang, S. Wang, and S. Liu, A Study on the Mechanical Properties of Polycrystalline Aluminum Nitride Based on Molecular Dynamics Simulation, *Mater. Today Nano*, **29**: 100581 (2025); https://doi.org/10.1016/j.mtnano.2025.100581
72. C.L. Cunha, T.C. Pimenta, and M.A. Fraga, Development and Applications of Aluminum Nitride Thin Film Technology, in *Thin Film Deposition-Fundamentals, Processes, and Applications* (IntechOpen: 2022); https://doi.org/10.5772/intechopen.106288
73. N. Afshar, M. Yassine, and O. Ambacher, A Comprehensive Review of Yttrium Aluminum Nitride: Crystal Structure, Growth Techniques, Properties, and Applications, *Sec. Semicond. Mater. Devices*, **12**: 1526968 (2025); https://doi.org/10.3389/fmats.2025.1526968
74. S. Saib and N. Bouarissa, Electronic Properties and Elastic Constants of Wurtzite, Zinc-Blende and Rocksalt AlN, *J. Phys. Chem. Solids*, **67**, No. 8: 1888–1892 (2006); https://doi.org/10.1016/j.jpcs.2006.05.007
75. N. Li, S.K. Yadav, J. Wang, X.-Y. Liu, and A. Misra, Growth and Stress-induced Transformation of Zinc Blende AlN Layers in Al-AlN-TiN Multilayers, *Sci. Rep.*, **5**: 18554 (2016); https://doi.org/10.1038/srep18554
76. J. Ruiz-González, G.H. Cocoletzi, and L. Morales de la Garz, Modeling the Electronic Structure and Stability of Three Aluminum Nitride Phases, *Revista Mexicana de Física*, **67**, No. 3: 343–350 (2021); https://doi.org/10.31349/revmexfis.67.343
77. V.M. Uvarov, Yu.V. Kudryavtsev, E.M. Rudenko, M.V. Uvarov, and S.A. Bespalov, Phase Composition and Electronic Structure of Aluminium Nitride AlN, *Metallofiz. Noveishie Tekhnol.*, **47**, No. 2: 125–134 (2025); https://doi.org/10.15407/mfint.47.02.0125
78. S. Uehara, T. Masamoto, A. Onodera, M. Ueno, O. Shimomura, and K. Takemura, Equation of State of the Rocksalt Phase of III–V Nitrides to 72 GPa or Higher, *J. Phys. Chem. Solids*, **58**, No. 12: 2093–2099 (1997); https://doi.org/10.1016/S0022-3697(97)00150-9
79. I. Gorczyca, N.E. Christensen, P. Perlin, I. Grzegory, J. Jun, and M. Bockowski, High Pressure Phase Transition in Aluminium Nitride, *Solid State Commun.*, **79**: 1033 (1991); https://doi.org/10.1016/0038-1098(91)90004-F
80. M. Ueno, A. Onodera, O. Shimomura, and K. Takemura, X-Ray Observation of the Structural Phase Transition of Aluminum Nitride Under High Pressure, *Phys. Rev.*

B, **45**, No. 17: 10123–10126 (1992);
https://doi.org/10.1103/PhysRevB.45.10123
81. L. Hultman, S., Benhenda, G. Radnoczi, J.E. Sundgren, J.E. Greene, and I. Petrov, Interfacial Reactions in Single-Crystal-TiN(100)/Al/Polycrystalline-TiN Multilayer Thin Films, *Thin Solid Films*, **215**, No. 2: 152–161 (1992);
https://doi.org/10.1016/0040-6090(92)90430-J
82. A.F. da Silva, N. Souza Dantas, J.S. de Almeida, R. Ahuja, and C. Persson, Electronic and Optical Properties of Wurtzite and Zinc-Blende TlN and AlN, *J. Cryst. Growth*, **281**, No. 1: 151-160 (2005);
https://doi.org/10.1016/j.jcrysgro.2005.03.021
83. P. Tsipas, S. Kassavetis, D. Tsoutsou, E. Xenogiannopoulou, E. Golias, S.A. Giamini, C. Grazianetti, D. Chiappe, A. Molle, M. Fanciulli, A. Dimoulas, Evidence for Graphite-Like Hexagonal AlN Nanosheets Epitaxially Grown on Single Crystal Ag(111), *Appl. Phys. Lett.*, **103**, No. 25: (2013);
https://doi.org/10.1063/1.4851239
84. S. Louhibi-Fasla, H. Achour, K. Kefif, and Y. Ghalem, First-Principles Study of High-Pressure Phases of AlN, *Phys. Procedia*, **55**: 324–328 (2014);
https://doi.org/10.1016/j.phpro.2014.07.047
85. C. Bacaksiz, H. Sahin, H.D. Ozaydin, S. Horzum, R.T. Senger, and F.M. Peeters, Hexagonal AlN: Dimensional-Crossover-Driven Band-Gap Transition, *Phys. Rev. B*, **19**, No. 8: 085430 (2015);
https://doi.org/10.1103/PhysRevB.91.085430
86. Q. Peng, X. J. Chen, S. Liu, and S. De, Mechanical Stabilities and Properties of Graphene-Like Aluminum Nitride Predicted from First-Principles Calculations, *RSC Adv.*, **3**: 7083–7092 (2013);
https://doi.org/10.1039/C3RA40841H
87. T.T. Yen, T. Hirasawa, P.K. Wright, A.P. Pisano, and L. Lin, Corrugated Aluminum Nitride Energy Harvesters for High Energy Conversion Effectiveness, *J. Micromech. Microeng.*, **21**: 085037 (2011);
https://doi.org/10.1088/0960-1317/21/8/085037
88. G. Bu, D. Ciplys, M. Shur, L.J. Schowalter, S. Schujman, and R. Gaska, Surface Acoustic Wave Velocity in Single-Crystal AlN Substrates. *IEEE Trans. Ultrason. Ferroelectr. Freq. Control*, **53**: 251–254 (2006);
https://doi.org/10.1109/tuffc.2006.1588412
89. T.M. Hartnett, S.D. Bernstein, E.A. Maguire, and R.W. Tustison, Optical Properties of ALON (Aluminum Oxynitride), *Proc. SPIE*, **3060**: 284–295 (1997);
https://doi.org/10.1117/12.277053
90. Z. Fan, Z. Qin, Z. Sun, and H. Wu, Broad Spectrum Detector Based on AlN Crystal, *J. Phys. Conf. Ser.*, **2350**: 012013 (2022);
https://doi.org/10.1088/1742-6596/2350/1/012013
91. H. Liu, P.-F. Shao, S.-L. Chen, T. Tao, Y. Yan, Z.-L. Xie, B. Liu, D.-J. Chen, H. Lu, R. Zhang, and K. Wang, Pit Density Reduction for AlN Epilayers Grown by Molecular Beam Epitaxy Using Al Modulation Method, *Chin. Phys. B*, **33**: 106801 (2024);
https://doi.org/10.1088/1674-1056/ad7671
92. M.K. Sandager, C. Kjelde, and V. Popok, Growth of Thin AlN Films on Si Wafers by Reactive Magnetron Sputtering: Role of Processing Pressure, Magnetron Power and Nitrogen/Argon Gas Flow Ratio, *Crystals*, **12**, No. 10: 1379 (2022);
https://doi.org/10.3390/cryst12101379
93. K. Bespalova, G. Ross, S. Suihkonen, and M. Paulasto-Krцckel, Metalorganic Chemical Vapor Deposition of AlN on High Degree Roughness Vertical Surfaces for MEMS Fabrication, *Adv. Electron. Mater.*, **10**, No. 4: 2300628 (2024);
https://doi.org/10.1002/aelm.202300628

94. M. Muhammed, M. Javidani, T.E. Sadrabadi, M. Heidari, T. Levasseur, and M. Jahazi, A Comprehensive Review of Cathodic Arc Evaporation Physical Vapour Deposition (CAE-PVD) Coatings for Enhanced Tribological Performance, *Coatings*, **14**, No. 3: 246 (2024); https://doi.org/10.3390/coatings14030246
95. R. Badis, J. Camus, A. Ayad, M. Rammal, R. Zernadji, N. Rouag, M. Abdou, and D. Hetero, Epitaxial Growth of AlN Deposited by DC Magnetron Sputtering on Si(111) Using a AlN Buffer Layer, *Coatings*, **11**, No. 9: 1063 (2021); https://doi.org/10.3390/coatings11091063
96. T.H. Kim and G.Y. Yeom, A Review of Inductively Coupled Plasma-Assisted Magnetron Sputter System, *Appl. Sci. Converg. Technol.*, **28**: 131–138 (2019); https://doi.org/10.5757/ASCT.2019.28.5.131
97. R.P. Martinho, F.J.G. Silva, R.J.D. Alexandre, and A.P.M. Baptista, TiB_2 Nanostructured Coating for GFRP Injection Moulds, *J. Nanosci. Nanotechnol*, **11**: 5374–5382 (2011); https://doi.org/10.1166/jnn.2011.3772
98. P. Borowski and J. Myśliwiec, Recent Advances in Magnetron Sputtering: From Fundamentals to Industrial Applications, *Coatings*, **15**, No. 8: 922 (2025); https://doi.org/10.3390/coatings15080922
99. A. Iqbal, K. Chaik, G. Walker, A. Iacopi, F. Mohd-Yasin, and S. Dimitrijev, RF Sputtering of Polycrystalline (100), (002), and (101) Oriented AlN on an Epitaxial 3C-SIC (100) on Si (100) Substrate. *J. Vac. Sci. Technol. B*, **32**: 06F401 (2014); https://doi.org/10.1116/1.4900418
100. A. Iqbal and F. Mohd-Yasin, Reactive Sputtering of Aluminum Nitride (002) Thin Films for Piezoelectric Applications: A Review, *Sensors*, **18**: 1797 (2018); https://doi.org/10.3390/s18061797
101. V. Popov, M. Chirumamilla, T. Krekeler, M. Ritter, and K. Pedersen, Magnetron Sputter Grown AlN Nanostructures with Giant Piezoelectric Response toward Energy Generation, *ACS Appl. Nano Mater.*, **6**: 8849-8856 (2023); https://doi.org/10.1021/acsanm.3c01250
102. L. Behera, N. Pandey, and M. Gupta, Synthesis and Characterization of AlN Thin Films Deposited Using DC and RF Magnetron Sputtering, *AIP Conf. Proc.*, **2265**: 030310 (2020); https://doi.org/10.1063/5.0017482
103. T.A. Edison, Art of plating one material with another, MKI, C23C14/325, Patent US526147A (Published 18.09.1894).
104. *Handbook of Vacuum Arc Science and Technology* (Eds. R.L. Boxman, D.M. Sanders, and P.J. Martin) (Park Ridge, NJ: Noyes Publications: 1995).
105. *Handbook of Plasma Immersion Ion Implantation and Deposition* (Ed. A. Anders) (John Wiley and Sons, Inc.: 2000).
106. D.M. Sanders and A. Anders, Review of Cathodic arc Deposition Technology at the Start of the new Millennium, *Surf. Coat. Technol.*, **133–134**: 78–90 (2000); https://doi.org/10.1016/S0257-8972(00)00879-3
107. A.A. Andreev, L.P. Sablev, V.M. Shulaev, and S.N. Grigoriev, *Vacuum-Arc Devices and Coatings* (Kharkiv: NSC 'KIPT': 2005).
108. B. Druz, Y. Yevtukhov, and I. Zaritskiy, Diamond-Like Carbon Overcoat for TFMH Using Filtered Cathodic Arc System with Ar-Assisted Arc Discharge, *Diamond Relat. Mater.*, **14**: 1508–1516 (2005); https://doi.org/10.1016/j.diamond.2005.04.007
109. Z. Liu, M. Song, Z. Wang, W. Yang, Y. Dong, Q.Sun, and Q. Zhou, Effects of Anode Evaporation Process on the Anode Sheath Characteristics in Vacuum Arc Plasma,

J. Phys. D: Appl. Phys., **58**: 115201 (2025);
https://doi.org/10.1088/1361-6463/ad7c5c
110. A. Anders, Ion Charge State Distribution of Vacuum Arc Plasmas: The Origin of Species, *Phys. Rev. E*, **55**, No. 1: 969–981 (1997);
https://doi.org/10.1103/PhysRevE.55.969
111. E. Byon and A. Anders, Ion Energy Distribution Functions of Vacuum Arc Plasmas, *J. Appl. Phys.*, **93**, No. 4: 1899–1906 (2003);
https://doi.org/10.1063/1.1539535
112. I.I. Beilis, The Phenomenon of a Cathode Spot in an Electrical Arc: The Current Understanding of the Mechanism of Cathode Heating and Plasma Generation, *Plasma*, **7**, No. 2: 329–354 (2024);
https://doi.org/10.3390/plasma7020019
113. R.L. Boxman and S. Goldsmith, Macroparticle Contamination in Cathodic Arc Coatings: Generation, Transport and Control, *Surf. Coat. Technol.*, **52**: 39–50 (1992);
https://doi.org/10.1016/0257-8972(92)90369-L
114. *Handbook of Vacuum Arc Science and Technology. Fundamentals and Applications* (Eds. R.L. Boxman, D.M. Sanders, and P.J. Martin) (Park Ridge, NJ: Noyes Publications: 1996).
115. A. Anders, A Review Comparing Cathodic Arcs and High Power Impulse Magnetron Sputtering (HiPIMS), *Surf. Coat. Technol.*, **257**: 308–325 (2014);
http://doi.org/10.1016/j.surfcoat.2014.08.043
116. R. Vladoiu, M. Tichý, A. Mandes, V. Dinca, and P. Kudrna, Thermionic Vacuum Arc—A Versatile Technology for Thin Film Deposition and Its Applications, *Coatings*, **10**, No. 3: 211 (2020);
https://doi.org/10.3390/coatings10030211
117. A. Shpak, E. Rudenko, I. Korotash, V. Semenyuk, V. Odinokov, G. Pavlov, and V. Sologub, Plasma Source of Low-Temperature Formation of Metal-Catalyst Nanoclusters, *Nanoindustriya (Nanoindustry)*, **4**: 12–15 (2009).
118. L. Osipov, E. Rudenko, V. Semenyuk, I. Korotash, V. Odinokov, G. Pavlov, and V. Sologub, Highly Effective Source of Low Temperature Deposition of Films and Coatings, *Nanoindustriya (Nanoindustry)*, **2**: 4–7 (2010).
119. I. Korotash, V. Odinokov, G. Pavlov, E. Rudenko, D. Polotsky, V. Semenyuk, and V. Sologub, A Plant for Nanostructures Formation, *Nanoindustriya (Nanoindustry)*, **4**: 14–19 (2010).
120. I. Korotash, V. Odinokov, G. Pavlov, D. Polotsky, E. Rudenko, V. Semenyuk, and V. Sologub, Formation of Carbon Nanostructures in a Single Technological Cycle, *Nanoindustriya (Nanoindustry)*, **1**: 10–14 (2011).
121. V.F. Semenyuk, E.M. Rudenko, I.V. Korotash, L.S. Osipov, D.Yu. Polotskiy, K.P. Shamray, V.V. Odinokov, G.Ya. Pavlov, and V.A. Sologub, Unitized Ion-Plasma Processing Equipment for Fabrication of Nanostructures, *Metallofiz. Noveishie Tekhnol.*, **33**, No. 2: 223–231 (2011).
122. V.F. Semenyuk, V.F. Virko, I.V. Korotash, L.S. Osipov, D.Yu. Polotsky, E.M. Rudenko, V.M. Slobodyan, and K.P. Shamrai, Controlling Parameters Determining Technological Properties of a Helicon Discharge System, *Problems Atomic Sci. Technol.*, **4**, No. 86: 179–182 (2013).
123. E.M. Rudenko, I.V. Korotash, V.F. Semenjuk, and K.P. Shamraj, Plant for Precision Ionic-Plasma Formation of Carbon Nanotubes in the United Vacuum-Technological Cycle, *Nauka Innov.*, **5**, No. 5: 5–8 (2009);
https://doi.org/10.15407/scin5.05.005
124. E.M. Rudenko, I.V. Korotash, V.F. Semenjuk, and K.P. Shamraj, Vacuum-Plasma Module for the Forming of Structure Element Base of Nanoelectronics and Micro-

energetics, *Nauka Innov.*, **6**, No. 3: 36–38 (2010);
https://doi.org/10.15407/scin6.03.036
125. E.M. Rudenko, V.Ye. Panarin, P.O. Kyrychok, M.Ye. Svavilnyi, I.V. Korotash, O.O. Palyukh, D.Yu. Polotskyi, and R.L. Trishchuk, Nitriding in a Helicon Discharge as a Promising Technique for Changing the Surface Properties of Steel Parts, *Prog. Phys. Met.*, **20**, No. 3: 485–501 (2019);
https://doi.org/10.15407/ufm.20.03.485

Received / Final version
01.03.2026 / 01.06.2026

Е.М. Руденко[1], *І.В. Короташ*[1], *М.В. Дякін*[1], *Д.Ю. Полоцький*[1],
С.А. Беспалов[1], *О.В. Гамалій*[2], *Н.В. Гамалій*[3], *В.А. Дехтяренко*[1,4]
[1] Інститут металофізики ім. Г.В. Курдюмова НАН України,
бульв. Академіка Вернадського, 36, 03142 Київ, Україна
[2] Державний науково-дослідний інститут авіації,
вул. Казарменна, 6, 01135 Київ, Україна
[3] Центральний науково-дослідний інститут озброєнь і військової техніки
Збройних Сил України,
просп. Повітряних сил України, 28, 03049 Київ, Україна
[4] Інститут електрозварювання ім. Є.О. Патона НАН України,
вул. Казимира Малевича, 11, 03150 Київ, Україна

НІТРИД АЛЮМІНІЮ ЯК ПЕРСПЕКТИВНИЙ БАГАТОФУНКЦІОНАЛЬНИЙ МАТЕРІАЛ.
Ч. 1. Властивості, кристалічна структура та технології виготовлення

Досліджено перспективний матеріал серед нітридів III групи, а саме нітриду Алюмінію (AlN), який завдяки своїм унікальним властивостям активно застосовується у промисловості. Охарактеризовано його основні фізико-механічні властивості та напрями використання (в акустичних, електронних та оптичних пристроях). На основі термодинамічних розрахунків визначено, що вільна енергія Ґіббса для окиснення металевого алюмінію до утворення сполуки Al_2O_3 є нижчою, і, відповідно, він активніше взаємодіє з киснем, аніж з азотом. Для активації реакції алюмінію з азотом, згідно з рівнянням Вант-Гоффа, парціальний тиск азоту має значно переважати тиск кисню і лише в такому випадку алюміній реагує переважно з азотом, утворюючи хімічну сполуку AlN. Розглянуто відомі шляхи зменшення негативного впливу кисню на процес утворення нітриду Алюмінію. Представлено основні методи одержання нітриду Алюмінію, зокрема тонких плівок, визначено їхні основні переваги та недоліки. Показано, що за основним механізмом хімічної реакції для вихідних компонентів методи одержання поділяють на шість комплексних груп. Визначено, що залежно від умов формування нітрид Алюмінію може бути в чотирьох модифікаціях: структура типу вюртциту з шириною забороненої зони у 6,2 еВ; структура типу шаруватої гексагональної з шириною забороненої зони у 3,44 еВ; структура типу цинкової обманки (сфалериту) з шириною забороненої зони у 3,24 еВ; структура типу кам'яної солі із шириною забороненої зони у 4,04 еВ. Проаналізовано особливості зазначених модифікацій AlN.

Ключові слова: нітрид Алюмінію, технології виготовлення, кристалічна структура, тонкоплівкові покриття, фізико-механічні властивості.